Essential Readings in Light Metals: Electrode Technology for Aluminum Production.
Edited by Alan Tomsett and John Johnson.

CHEMICAL DEGRADATION MAP FOR SODIUM ATTACK IN REFRACTORY LININGS

K.Tschöpe[1], J.Rutlin[2], T.Grande[1,3]
[1]Department of Materials Science and Engineering; Norwegian University of Science and Technology, N-7491 Trondheim
[2]HydroAluminium As, N-6882 Øvre Årdal
[3]Corresponding author: tor.grande@material.ntnu.no

Abstract

Here we show by autopsies of spent pot linings that the degradation of the refractory lining in aluminum reduction cells is governed by sodium transport into the lining. The chemical reactions caused by sodium infiltration are qualitatively explained by the construction of a chemical degradation map. The degradation map corresponds to a predominance phase diagram showing the stable compounds present as a function of SiO_2/Al_2O_3 ratio in the refractory lining and the amount of sodium infiltrated in the lining. We demonstrate that the degradation map is a useful tool for the evaluation of autopsies of spent pot linings and the prediction of the mineralogical composition of the spent pot lining.

Introduction

The cathode lining, with the characteristic sequence of layers of different materials, is one of the most important parts in Hall-Héroult cells to ensure an appropriate service life. Layers of refractories are installed below the carbon cathode to maintain the desired heat balance and to protect the insulation bricks underneath against higher temperatures and chemical attack [1]. The most common refractory materials are located in the Al_2O_3-SiO_2 system. These materials are usually called aluminosilicates and they are distinguished by their alumina content [2]. If the content is between 10-45 wt% it is referred as "chamotte" group and > 45 wt% it is referred to as high alumina bricks. Cristoballite (SiO_2), mullite ($3Al_2O_3 \cdot 2SiO_2$) and a silica rich glass are the dominating phases in chamotte bricks. The protection of the subsequent high porous insulation layer(s) against chemical degradation is more important than the refractoriness of the materials [2].

However, the refractory material cannot completely withstand the permanent chemical attack. The percolating molten electrolyte or bath reacts and destroys the lining material immediately after cell start-up and continues relative intensively during the early stage of operation. With increasing diffusion depth the penetration rate slows down, but proceeds the entire lifetime, because the electrolyte continues to percolate through the cathode [3]. This attack leads to significant mineralogical transformations of all lining materials in contact with the molten fluorides [2-7]. Over time this will have an impact on material performances [8] and thus on the life span of the cell or in the worst case it will cause a complete pot failure.

To prevent this it is important to gain more knowledge about cell lining and the material stability. Common ways to investigate the chemical as well as the physical properties of spent pot linings are the so called autopsies. Autopsies are done after failures or normal cell shutdowns and the observed order of materials has been assumed to reflect the situation before the pot was taken out of service. Earlier work done by the authors [9] has shown that the common physical appearance or sequence of layered structure is not reflecting the conditions under operation. It is more likely a combination of operation and the crystallisation of molten constituents proposed to be present below the cathode during operation.

The current understanding of the degradation process is, that besides the well known attack of fluoride melt [2-6, 10], the metallic sodium vapor is the first attacking agent in the cathode lining and is the major species acting at the reaction front [9, 11]. The importance of reaction with sodium in the refectory lining is confirmed by the experimental data reported here giving evidence for the presence of only sodium at the reaction front.

To predict mineralogical changes in aluminosilicate pot linings Schøning et al. [2] presented a degradation map of the so-called "wet attack" by the molten electrolyte (represented by molten NaF). NaF was shown to react with the lining materials and the mineralogical phase composition depends on the silica to alumina ratio of the raw lining material. The phase composition as a function of the silica content present in the lining is illustrated in Figure 1, which is defined by 6 quaternary regions, where β-alumina, nepheline and albite are identified as secondary phases formed due to the reaction with NaF.

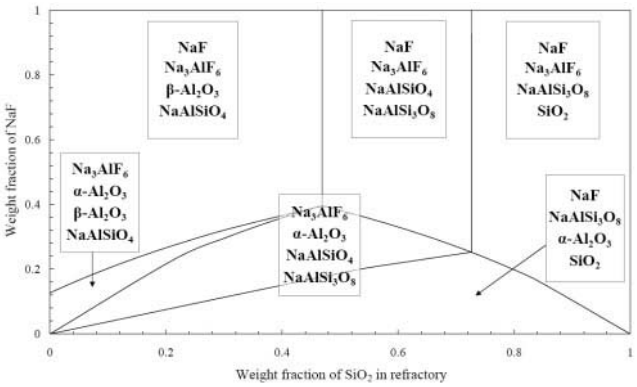

Figure 1: Phase compositions due to chemical reaction between aluminosilicate materials and sodium fluoride. The phase composition is given as a function of the silica content in the refractory material and the weight fraction of NaF relative to the amount of aluminosilicate material [2].

The present work is a continuation of the previous consideration of the chemistry of the deterioration of the refractory lining and the corresponding degradation map by sodium vapor attack, which is the so-called "dry" attack. The stable compounds formed at the specific degradation conditions of aluminosilicate refractories are summarized in a predominance phase diagrams or degradation map. Finally, we illustrate the usefulness of the degradation map in the analysis of spent pot linings.

Experimental

Autopsies and Sampling

Cathode autopsies and laboratory tests of spent pot lining materials from shut down cells have been performed to document the status of the lining and possibly to find the reasons for pot failures. In this paper the analysis of the cross section of refractory linings from three cells operated for 1569, 1767 and 2168 days are reported. The cathode cell lining consisted of, beside the graphitized carbon cathode, a sequence of aluminosilicate refractories and common insulation materials at the bottom with a thickness ratio of 1:1 or 3:1. Material sampling from the spent pot lining were carried out by hand. Analyses were performed for the materials through the cross section from un-reacted materials to the salt lense above the converted refractory bricks. The samples were cut by circular diamond saw, cooled with water and dried in a furnace at 100 °C for 48 h. The samples discussed in the present report were taken from the borderline between the deteriorated/transformed section and the virgin/intact material. This intersection is called reaction front in the following, see Figure 2.

EPMA

Line scan and mapping of the element composition were performed by electron microprobe analysis (EMPA) using a JXA-8500F Hyperprobe JOEL (EPMA/WDS) apparatus. The reaction front samples were embedded into epoxy and polished by hand, to avoid further contact of liquids which might react with the materials. After the polish the samples were coated with carbon to reduce the problems with charging of the samples. The electron beam spot size was broadened to 30 µm to avoid Na evaporation. The sample source, appearance as well as the final preparation state is shown in Figure 2.

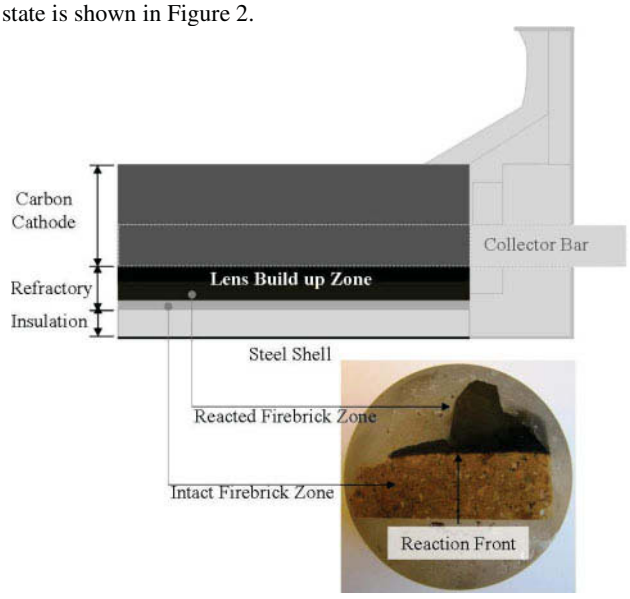

Figure 2: The position of the sample analysed by EMPA and an optical image of the cross section near the reaction front (un-reacted material red, reacted material black).

Powder X-Ray diffraction

Samples above the reaction front up to the carbon cathode surface were crushed in a ball mill (Retsh MM2000) for 2 minutes and sieved to less than 63 µm. The powder was than mounted in a silicon sample holder for powder X-ray diffraction analysis. Qualitative phase composition was investigated by powder X-ray diffraction using a Bruker AXS D8 Focus X-ray diffractometer with a LynxEye detector. The step size was 0.02° with a counting time of 0.5 s in the 2-Theta range of 5° to 80°. High resolution diffractograms were also recorded using a Bruker AXS D8 Advance X-ray diffractometer with a Våntec-1 detector (step size of 0.016°, counting time of 2.0 s, 2-Theta range 6° to 120°).

Results

Element mapping at the reaction front

The line scans and area mappings across the reaction front from three different cells were recorded by EPMA. The results are shown in Figure 3 and 4. The content of the major components Si, Al, O, F and Na and the minor elements Ca, K, Mg and Fe were recorded. The diagrams in Figure 4 show the content of Na and F in wt% over the distance of 2 mm across the intersection. For each cell the concentration gradient of sodium is clearly evident. At the reaction front the sodium gradient is particularly steep and the sodium content decreases rapidly from 10-14 wt% to approximately 1-2 wt%, which corresponds to the initial impurity level in the refractory materials. Interestingly, there is no corresponding gradient in the fluorine content across the reaction front, and fluorine concentration is almost zero across the entire reaction zone. Area mapping of the same region indicated no F and the Na front can clearly be observed, see Figure 3. This implies that the attacking agent at the reaction front is sodium and that the deterioration mechanism in this area is not a combination of “wet" (NaF) and “dry" (Na (g)) attack. Na (g) penetrates faster than the bath components. Since there is no material which is stable in contact with Na (g) the degradation will proceed [11]. In previous reports it has been proposed that the diffusion is slowed down due to the formation of a viscous liquid. Here we support the previous suggestions of a viscous layer, but we show that this viscous layer at the reaction front contains only sodium aluminium silicates [9].

Phase composition

The phases found in the spent pot lining were in line with what has been found in most autopsies [12, 13]. The main phases in the carbon cathode were cryolite, sodium fluoride, β-alumina and a minor amount of calcium fluoride (CaF_2). Underneath the cathode or in the so called lens build up zone α - and ß-alumina (α/ß-Al_2O_3), cryolite (Na_3AlF_6), sodium fluoride (NaF), nepheline ($NaAlSiO_4$) and silicon (Si) were detected. In the reacted firebrick zone α-, ß -alumina and cryolite disappeared. Finally close to the reaction front only nepheline ($NaAlSiO_4$) and silicon (Si) could be detected in addition to an amorphous phase. The glassy phase does mainly consist of a sodium aluminosilicate glass. The presence of the silicon at the reaction front confirms the reducing conditions due to the presence of Na.

Discussion

Degradation Map for the "Dry" Attack

Schøning *et al.* considered the chemical stability of some refractory materials in sodium-rich environments [2, 11]. The main important conclusion was that sodium has a strong reductive nature and deteriorates all exposed aluminosilicate bricks. It is also well known that sodium penetrates faster through the cathode carbon block than fluoride melts [14]. Our previous [9] and present examination of the reaction front have shown that this scenario will continue through the entire cell cross section. Thus metallic sodium vapor will also be the first attacking agent degrading the pristine refractory material further down in the cell lining. This is evidenced by the cross section of the relatively old cells shown in Figure 3 and 4. Therefore it is important to consider a degradation map for the so called "dry" attack by metallic sodium vapor (Figure 5).

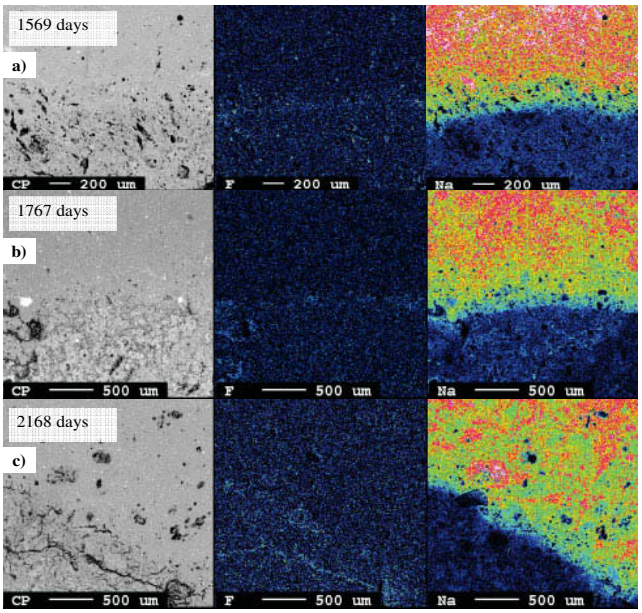

Figure 3: Results of the area scan across the interface between reacted firebrick and non reacted firebrick of 3 different pot ages; plot a) is published before [9]. The lighter the colour the higher is the amount of the detected element. Here blue means zero and red highest concentration.

A unified approach of corrosion maps (we are using the term degradation map) taking both reacting agents (molten NaF and metallic Na) on alumino-silicates into account was proposed by Pelletier *et al.* [12, 13]. They assumed that all the sodium was oxidized atmospherically to Na_2O. The reaction pattern is shown by Reaction (1). The degradation path will vary dependent on the NaF: Na_2O ratio.

$$Na_2O + NaF + AlF_3 + [\text{aluminosilicate refractories}] = [\text{Na-Al-F compounds}] + [\text{Al-Si-Na-O compounds}] \quad (1)$$

The complete oxidation of sodium is questionable since elemental silicon droplets found in the reaction front have shown that the deterioration takes part at reducing conditions, where sodium metal reduces silica in the lining to Na_2O and Si metal. Thermodynamically, sodium works as a strong reducing agent with respect to the most oxides. Thus in this report the degradation map of metallic sodium vapor was established.

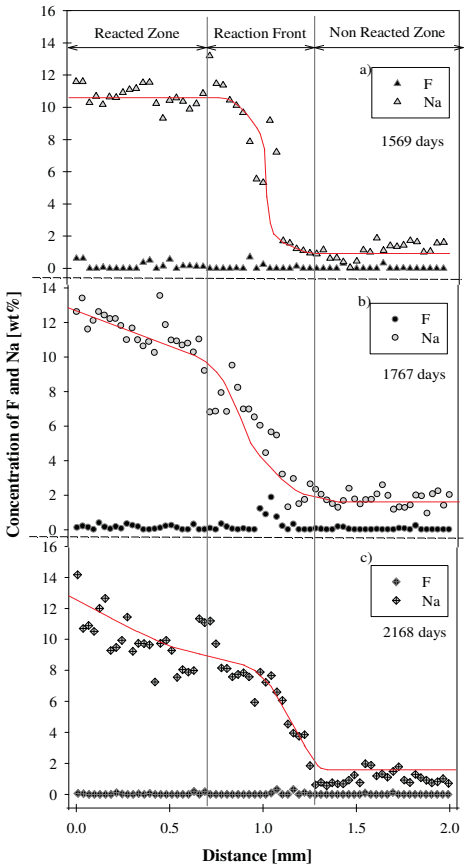

Figure 4: Results of the chemical analysis across the interface between reacted firebrick and intact firebrick of 3 different pot ages, plot a) is published before [9].

The map, shown in Figure 5, is significantly more complex with several stability regions. The degradation map or the phase diagram was constructed based on the thermodynamically possible Reactions (3) to (14) shown by the negative Gibbs energy, given in Table 1.

Table 1: Gibbs energies for Equations (3) to (14)

Equation number	ΔG^o_{1100K} [kJ]	Equation number	ΔG^o_{1100K} [kJ]
(3)	-28.00	(9)	-135.54
(4)	-60.74	(10)	-67.60
(5)	-71.16	(11)	-48.23
(6)	-34.46	(12)	-73.40
(7)	-120.08	(13)	-81.06
(8)	-9.17	(14)	-81.63

The first Reaction (2) takes place at the interface between the molten electrolyte and Al metal [1].

$$3\ NaF\ (l) + Al\ (l) = 3\ Na\ (\text{in carbon}) + AlF_3\ (l) \quad (2)$$

Due to Reaction (2) [4] metallic Na will continuously be produced at the bath/metal interface and penetrates through the carbon cathode. Underneath the carbon cathode sodium reacts and reduces the oxide materials present in the refractory lining, to form sodium aluminates like β-alumina, $NaAlO_2$, nepheline and silicon (3-7). At higher SiO_2 contents albite ($NaAlSi_3O_8$) will be produced at the expense of nepheline ($NaAlSiO_4$). Since both of these two reaction products are not stable in contact with sodium, they can further react with sodium according to Reactions (8) and (10). Albite is more unstable than nepheline.

However, the reduction of these reaction products of the deteriorated lining is disadvantageous with respect to maintain a viscous penetration barrier, which retards further penetration [2]. The silicon will precipitate as small accumulations in the reacted refractory layer and will appear as bright precipitates [11].

$$Na\ (g) + 14/3\ Al_2O_3\ (s) = NaAl_9O_{14}\ (s) + 1/3\ Al\ (l) \quad (3)$$
(ß-alumina)

$$Na\ (g) + 3\ Al_2O_3\ (s) + 1/4\ SiO_2\ (s) = 1/2\ Na_2Al_{12}O_{19}\ (s) + 1/4\ Si\ (s) \quad (4)$$
(ß"-alumina)

$$Na\ (g) + 9/2\ Al_2O_3\ (s) + 1/4\ SiO_2\ (s) = NaAl_9O_{14}\ (s) + 1/4\ Si\ (s) \quad (5)$$

$$Na\ (g) + 1/2\ Al_2O_3\ (s) + ¼\ SiO_2\ (s) = NaAlO_2\ (s) + 1/4\ Si\ (s) \quad (6)$$

$$Na\ (g) + 1/2\ Al_2O_3\ (s) + 5/4\ SiO_2\ (s) = NaAlSiO_4\ (s) + 1/4\ Si\ (s) \quad (7)$$

$$Na\ (g) + 3/4\ NaAlSiO_4\ (s) = 3/4\ NaAlO_2\ (s) + 1/2\ Na_2SiO_3\ (s) + 1/4\ Si\ (s) \quad (8)$$

$$Na\ (g) + 1/2\ Al_2O_3\ (s) + 13/4\ SiO_2\ (s) = NaAlSi_3O_8\ (s) + 1/4\ Si\ (s) \quad (9)$$

$$Na\ (g) + 3/8\ NaAlSi_3O_8\ (s) = 3/8\ NaAlSiO_4\ (s) + 1/2\ Na_2SiO_3\ (s) + 1/4\ Si\ (s) \quad (10)$$

$$Na\ (g) + 1/2\ SiO_2\ (s) = 1/4\ Na_4SiO_4\ (s) + 1/4\ Si\ (s) \quad (11)$$

$$Na\ (g) + 3/4\ SiO_2\ (s) = 1/2\ Na_2SiO_3\ (s) + 1/4\ Si\ (s) \quad (12)$$

$$Na\ (g) + 5/4\ SiO_2\ (s) = 1/2\ Na_2Si_2O_5\ (s) + 1/4\ Si\ (s) \quad (13)$$

$$Na\ (g) + 19/12\ SiO_2\ (s) = 1/6\ Na_6Si_8O_{19}\ (s) + 1/4\ Si\ (s) \quad (14)$$

The degradation reactions are summarized in the degradation map shown in Figure 5. The coexisting phases in the stability regions in this predominance diagram are summarized in Table 2.

Interpretation of Autopsies using the Degradation Map

The degradation maps can be used to predict and interpret experimental investigations of spent pot lining. The starting point of the degradation path is the initial lining composition, corresponding to the silica content neglecting the trace amount of other oxides in the lining. For instance the chemical composition of a common chamotte brick (e.g. Alubar1100) can be 68 wt% SiO_2 and 26 wt% Al_2O_3, which gives a normalized weight ratio of 72:28. Thus the initial composition of the lining corresponds to 72 wt% SiO_2 and 28 wt% Al_2O_3. For comparison, a second lining composition of 68 wt% SiO_2 and 32 wt% Al_2O_3 is also used. The

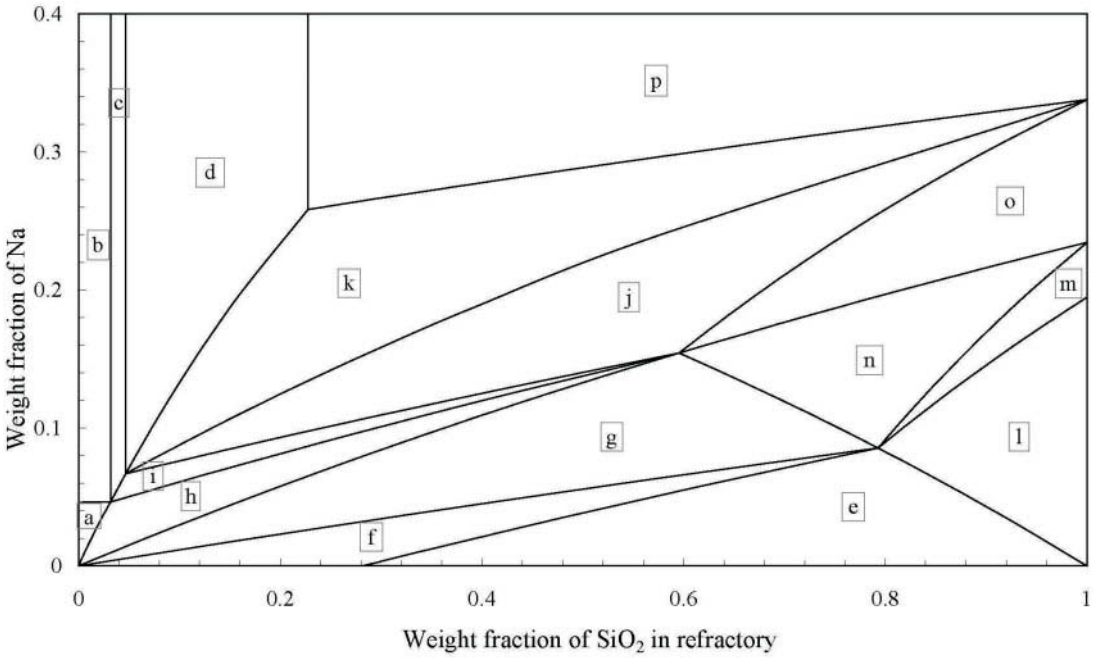

Figure 5: Phase composition due to chemical reaction between aluminosilicate materials and sodium. The phase composition is given as a function of the silica content in the refractory material and the weight fraction of Na relative to the amount of aluminosilicate refractories. The coexisting phases of each domain are shown in Table 2.

two lining compositions are marked as vertical lines in Figure 6.

Table 2: Coexisting phases for the different regions shown in Figure 5.

Region number	Coexisting phases		Region number	Coexisting phases
a	α-Al_2O_3		f	α-Al_2O_3
	ß-Al_2O_3			$Al_6Si_2O_{13}$
	Al			$NaAlSi_3O_8$
	Si			Si
b	ß-Al_2O_3		g	α-Al_2O_3
	Na			$NaAlSiO_4$
	Al			$NaAlSi_3O_8$
	Si			Si
c	ß-Al_2O_3		h	α-Al_2O_3
	ß”-Al_2O_3			$NaAlSiO_4$
	Na			ß-Al_2O_3
	Si			Si
d	$NaAlO_2$		i	ß”-Al_2O_3
	ß”-Al_2O_3			$NaAlSiO_4$
	Na			ß-Al_2O_3
	Si			Si
e	SiO_2		j	ß”-Al_2O_3
	$Al_6Si_2O_{13}$			$NaAlSiO_4$
	$NaAlSi_3O_8$			Na_2SiO_3
	Si			Si
k	$NaAlO_2$		n	$Na_2Si_2O_5$
	Na_2SiO_3			$NaAlSiO_4$
	ß”-Al_2O_3			$NaAlSi_3O_8$
	Si			Si
l	SiO_2		o	$Na_2Si_2O_5$
	$Na_6Si_8O_{19}$			$NaAlSiO_4$
	$NaAlSi_3O_8$			Na_2SiO_3
	Si			Si
m	$Na_2Si_2O_5$		p	$NaAlO_2$
	$Na_6Si_8O_{19}$			Na
	$NaAlSi_3O_8$			Na_2SiO_3
	Si			Si

The sodium content in the spent pot lining has to be established by chemical analysis. An average Na content corresponding to 11 wt% can be found near the reaction front in Figure 4a), and this sodium content is marked by a horizontal line in Figure 6, as well as a second value of 16 wt% (for comparison).

The intersection between 11 wt% sodium and 72 wt% silica can be found in the stability region (n) in Figure 6, where α-Al_2O_3, $NaAlSiO_4$, $NaAlSi_3O_8$ and Si metal are the coexisting phases. This result can be verified by the comparison with the chemical analysis of the reaction front [9]. As expected, neither albite ($NaAlSi_3O_8$) nor α-Al_2O_3 was detected by XRD, since the former mineral normally does not crystallize and the latter is dissolved in the glass. Albite is present as amorphous or glassy phase in reacted refractory layers of shut down cells. $NaAlSiO_4$ and Si were the only detected crystalline phases, which show a good agreement with the proposed degradation map.

The reaction scheme of the degradation map can also be estimated by using a ternary phase diagram of the system Na_2O-Al_2O_3-SiO_2 as shown in Figure 7. This system can be divided into 11 Alkemade triangles, were each of them represents the three specific coexisting compounds. Since this diagram is made of oxides, the Na content has to be converted into Na_2O according to Reaction (15). The SiO_2 will be reduced by Na to form Na_2O and Si. This converting reaction is valid for regions in the degradation map were Si metal is produced (c-p). In region (a) and (b) Al as well as Na metal are produced in addition to Si, but since refractory compositions with silica contents up to 4.6 wt% are not common, the focus will be on Reaction (15).

$$4\ Na\ (g) + SiO_2\ (s) = 2\ Na_2O\ (s) + Si\ (s) \qquad (15)$$

We now start with the composition of 72 wt% SiO_2 and 28 wt% Al_2O_3 (15). The experimentally determined content of Na (g) is then used to convert the amount of silica to sodium oxide according to Reaction to (15). On the basis of mass balance calculations the remaining SiO_2, the initial alumina content and the produced sodium oxide gives a particular composition in the ternary phase diagram. The pristine refractory composition is located at the SiO_2-Al_2O_3 side and the Na_2O-Al_2O_3 join represents

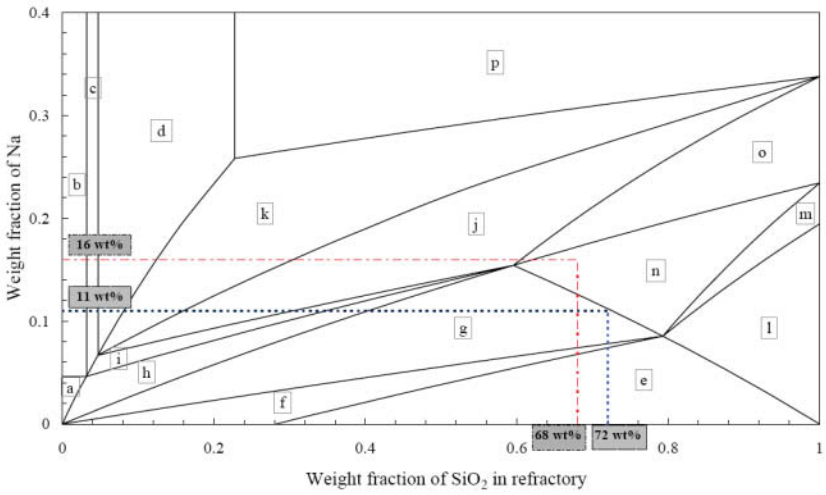

Figure 6: Redrawn from Figure 5 including two examples of initial refractory material compositions and corresponding Na contents.

the products, when all the silica is consumed. The straight line between the two points represents the path of sodium attack.

Here, 72 wt% SiO_2 can be fully converted into 84.13 wt% Na_2O and 15.87 wt% Al_2O_3, shown in the Na_2O-Al_2O_3-SiO_2 phase diagram in Figure 7 (green line). Dependent on the SiO_2/Al_2O_3 ratio of the raw refractory material the path will shift as shown by the red line for the case 68 wt% SiO_2 and 32 wt% Al_2O_3. The reactions during Na attack can be found by following the path, which crosses successive Alkemade triangles along the path. The resulting reactions correspond to the reactions summarized above.

The intersection of the vertical lines (72 wt% or 68 wt% SiO_2) with the horizontal line of 11 wt% in region (g) or with 16 wt% in region (n) in Figure 5 and 6 can be found as the points shown in Figure 7. Here, Reaction (15) is used to convert Na into Na_2O. It can clearly be seen that the points are appearing in the "right" Alkemade triangles, where the coexisting products (phases) correspond to the ones observed in the degradation map for "dry" attack.

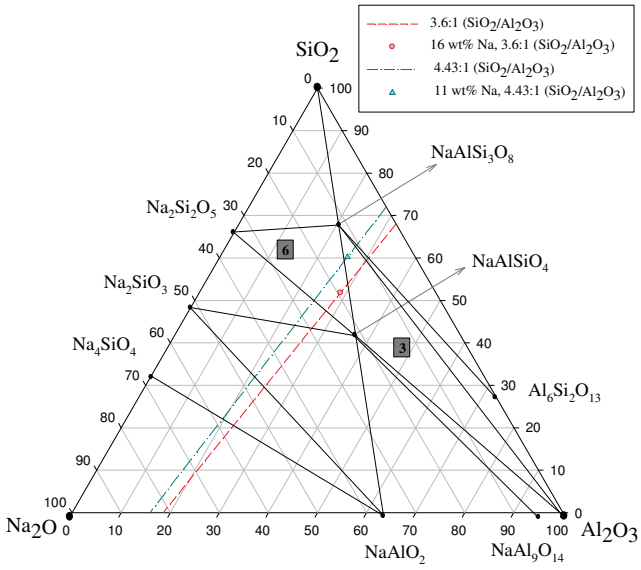

Fig. 7: Redrawn Na_2O-Al_2O_3-SiO_2 system [15] for easier implementation of the degradation path and results from the degradation map.

Conclusion

A complex degradation map of "dry" attack based on metallic sodium was established, inspired by the work of Schøning et al. [2]. The calculation was verified by a comparison with analytical results. Thus it is possible to predict mineralogical changes in the reaction front of aluminosilicate pot linings. The only requirement is the knowledge of the Na content and the initial refractory composition.

Acknowledgements

Hydro Primary Metal Technology and the Norwegian Research Council are acknowledged for financial support through the NRC project number 174276.

References

1. M. Sørlie and H. A. Øye, *Cathodes in Aluminium Electrolysis* (Düsseldorf, Germany: Aluminium Verlag, 2nd ed., 1994).

2. C. Schøning, T. Grande and O.-J. Siljan, *"Cathode Refractory Materials for Aluminium Reduction Cells"*, Light Metals (1999), pp. 231-238.

3. J. Rutlin and T. Grande, *"Fluoride Attack on Alumino-Silicate Refractories in Aluminium Electrolysis Cells"*, Light Metals (1997), pp. 295-301.

4. O.-J. Siljan, C. Schøning and T. Grande, "*State-of-the-Art Alumino-Silicate Refractories for Al Electrolysis Cells*", JOM, 54 (5) (2002), pp. 46-54, 63.

5. F. Brunk, *"Corrosion and Behaviour of Fireclay Bricks of Varying Chemical Composition Used in Bottom Lining of Reduction Cells"*, Light Metals (1994), pp. 477-482.

6. O.-J. Siljan, *"Sodium Aluminium Fluoride Attack on Alumino-Silicate Refractories"*, Dr.Ing.thesis, Department of Inorganic Chemistry, Norwegian Institute of Technology (1990).

7. O.-J. Siljan, T. Grande and Ch. Schøning, *"Refractories for Aluminium Electrolysis Cells."* Part I-IV, ALUMINIUM (77) (2001).

8. H.A. Øye, *"Property Changes of Cathode Lining Material During Cell Operation"*, Light Metals (1995), pp. 497-506.

9. K. Tschöpe, Ch. Schøning and T. Grande, *"Autopsies of Spent Pot linings- a Revised View"*, Light Metals (2009), pp 1085-1090.

10. J. Rutlin and T. Grande, *"Phase Equilibria in Subsystems of the Quarternary Reciprocal System Na_2O-SiO_2-Al_2O_3-NaF-SiF_4 AlF_3"*, J.Am.Ceram.Soc., 82 [9] (1999), pp. 2538-2544.

11. C. Schøning and T. Grande, *"The Stability of Refractory Oxides in Sodium-Rich Environments"*, JOM, 58 (2) (2006), pp. 58-61.

12. R. Pelletier et al., *"The Corrosion of Potlining Refractories: a Unified Approach"* JOM, 53 (8) (2001), pp. 18-22.

13. R. Pelletier and C. Allaire, *"Corrosion in Potlining Refractories: Effect of Cathode Material Interpreted Using a Unified Approach"*, JOM, 55 (11) (2003), pp. 58-62.

14. L.P. Lossius, P. Brilliot and H.A. Øye, *"Penetration and Chemical Reactions in Carbon Cathodes during Aluminium Electrolysis: 1. Laboratory Experiments"*, MET. TRANS. B PROCESS METALLURGY (24) (1993), pp. 75-89.

15. E.F. Osborn and A. Muan, *"Phase Equilibrium Diagrams of Oxide System"*, Am. Ceram. Soc. and the Edward Orton Jr. Ceramic Foundation (1960).